Modelling and Simulating Human Movement Neuromechanics

Massimo Sartori

Abstract Biological actuators are different from their mechatronic counterparts in terms of form and function. In this chapter, we discuss a data-driven neuromechanical model-based approach to estimate how muscles are neurally recruited as well as how they contribute to actuate multiple biological joints.

Human movement emerges from the coordinated interaction between the neuromuscular and the musculoskeletal systems (Enoka 2008). Despite knowledge of the mechanisms underlying movement neuromuscular and musculoskeletal functions, there currently is no relevant understanding of the neuro-mechanical interplay in the composite neuro-musculo-skeletal system. This represents a major challenge to the understanding of human movement, where the characterisation of mechanisms at one level, i.e., skeletal level, requires knowledge of mechanisms at the other levels, i.e., neuro-muscular (Enoka 2008; Sartori et al. 2017b).

This chapter proposes a neuromechanical modelling approach developed by the author and colleagues in the past years for the study of human movement neuromechanics. This is based on solving for how muscles are neurally recruited and for how they transfer mechanical forces to skeletal structures (Fig. 1).

1 Sampling α-Motor Neuron Discharges in Vivo

The motor unit is the actual biological interface between neural and musculoskeletal functions in humans and animals (Enoka and Pearson 2013). The 'α-motor neuron side' of the motor unit is the final common pathway of synaptic inputs produced in

M. Sartori (✉)
Department of Biomechanical Engineering, University of Twente, De Horst 2, Enschede 7522LW, NL, Netherlands
e-mail: m.sartori@utwente.nl

P. Beckerle et al. (eds.), *Novel Bioinspired Actuator Designs for Robotics*,
Studies in Computational Intelligence 888,
https://doi.org/10.1007/978-3-030-40886-2_2

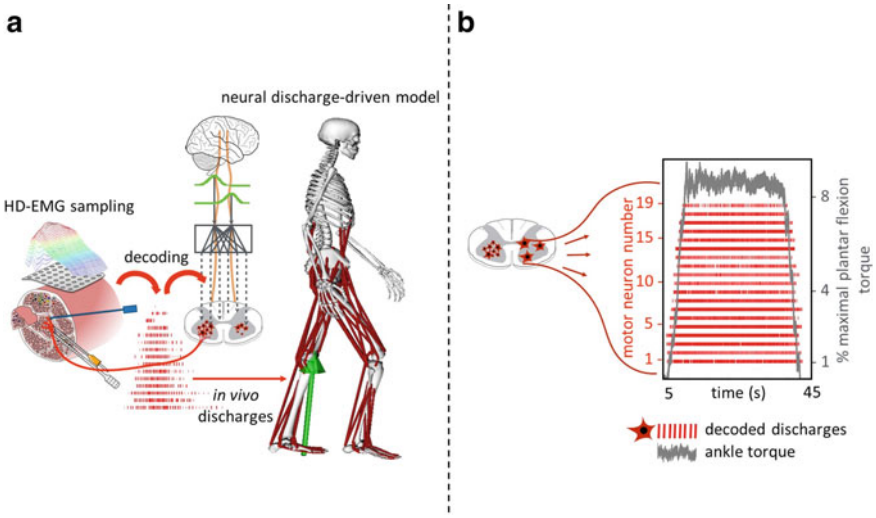

Fig. 1 High-density electromyograms (HD-EMGs) are recorded and decomposed into constituent motor unit discharges. This enables inferring spinal cord neural activity in vivo and non-invasively. Decoded discharges are used to drive forward neuro-musculo-skeletal models that can estimate a larger spectrum of neuromuscular mechanisms than is possible via signal-based techniques alone (**a**). Example spike trains decoded for 19 active motor units in the soleus muscle during isometric plantar flexion. The graph also shows the ankle plantar flexion torque generated during the task (**b**)

different areas of the nervous system and represents the optimal level for bridging the neuro-muscular 'knowledge gap' in movement.

In this context, advances in electromyography (EMG) are enabling discerning the activity of motor units from interferent EMGs data. This is helping understand how α-motor neurons receive synaptic input from spinal and supraspinal levels and regulate muscle activation (Bizzi et al. 2008; Farina and Negro 2015).

The α-motor neurons can be recorded from the intact moving human in vivo using soft-electronic skins; highly dense (HD) grids of electrodes that can be placed on the skin surface for recording HD-EMGs from a large number of muscle fibers simultaneously (Fig. 1a). This is possible because of the safe synaptic connection between a motor neuron and the innervated muscle fibers. As a result, there is a one to one relationship between action potential produced by an α-motor neuron and that generated by the innervated fibers. That is, each motor neuron action potential is transduced into a compound muscle fiber action potential that carries the same neural information. HD-EMGs carry this information in the form of an interferent signal, from which the underlying α-motor neuron discharges can be unmixed via deconvolution-based blind source separation (Farina et al. 2017). This provides the same feature that direct nerve interfacing extracts via implanted electrodes, i.e., nerve intrafascicular or epimysial electrodes. That is, it provides access to the time series of discharge events of populations of motor neurons, i.e., > 30 neurons per controlled muscle.

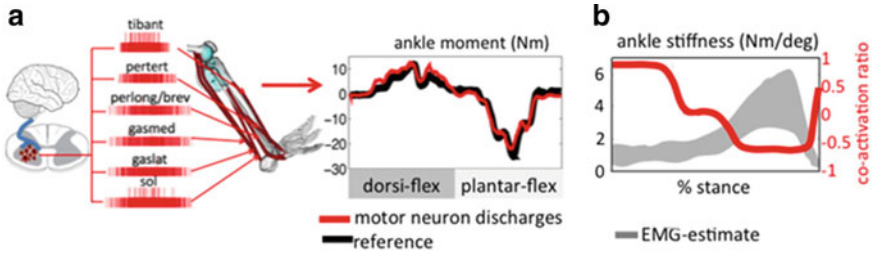

Fig. 2 Neural discharge-driven modelling. In vivo motor neuron cellular cumulative spike trains are decoded for muscles including tibialis anterior (tibant), peroneus tertius (pertert), brevis (perbrev), longus (perlong), gastricnemius medialis (gasmed), lateralis (gaslat), and soleus (sol). These drive forward musculoskeletal models enabling prediction of isometric ankle moment (**a**). Reference and predicted ankle joint stiffness via electromyography-driven modelling during locomotion. This data-model fusion framework shows how agonist–antagonist co-activation ratio varies from dominant dorsi flexors (+1; initial stance) to plantar flexors(−1; late stance) and regulates joint-equivalent stiffness (**b**)

We recently showed how multi-muscle spatial sampling and deconvolution of high-density fiber electrical activity could be used to decode accurate alpha-motor neuron discharges across five lumbosacral segments in the human spinal cord (Sartori et al. 2017a, b). This was achieved by recording HD-EMG from five ankle muscles using more than 250 recording sites (Fig. 2b). This provides a window into α-motor neuron pool activity and its distribution across the rostrocaudal axis of the spinal cord (Sartori et al. 2017a, b).

This information can be used to estimate motor unit anatomical properties including fiber diameter and fatiguability (Del Vecchio et al. 2017). This enables building motor unit-specific twitch models that can convert decoded α-motor neuron discharges into muscle activation profiles.

Moreover, complete motor neuron decoding potentially provides a window into the synaptic inputs converging onto these pools (Negro et al. 2016), thus enabling understanding the organization and connections in higher spinal neural networks (Fig. 2). Coherence analysis can be employed to determine the proportion of common and independent synaptic input converging to α-motor neuron pools (Farina and Negro 2015, Gogeascoechea et al. 2020). Dimensionality reduction techniques (Lee and Seung 1999), can be used to extract estimates of muscle modularity and synergies (Sartori et al. 2013b; Gonzalez-Vargas et al. 2015).

2 From α-Motor Neurons Discharges to Muscle–Tendon Force

Common neurophysiological analyses typically focus on the ‘motor neuron side’ with less emphasis on the ‘muscle fiber side’ and how its contractile dynamics contributes to motor control and function (Herzog 2014). However, human movement must be

understood with a linked perspective to motor neurons and muscle contractile properties simultaneously. It was shown that the difference between muscle isometric force to microstimulation and dynamic force during movement produced by the same microstimulation can be one order of magnitude different (Barbeau et al. 1999). Studies established that central nervous system (CNS) control strategies change across contraction types, i.e., lengthening, shortening or isometric (Duchateau and Enoka 2016). Furthermore, muscle contraction history dependence (not regulated by the CNS) can directly affect muscle excitation–contraction couplings, i.e., force enhancement following stretch can reach values of almost 50% of the corresponding isometric reference force (Herzog et al. 2015). These differences need to be accounted for via mechanistic models of the contribution of fiber contractile properties.

A possible way of doing this is via neural data-driven musculoskeletal modelling formulations (Sartori et al. 2016). Previous research demonstrated that this can effectively translate motor neuron discharges into multi-muscle coordinated force patterns resulting into net ankle joint moment (Sartori et al. 2017b).

This is a "predictive formulation" where cumulative spike trains (CSTs) decoded from all motor neurons active in the control of a specific muscle directly drive muscle fibers and series elastic tendons, i.e., muscle–tendon units (MTUs, Fig. 2). This modelling formulation comprises six main components (Sartori et al. 2012a, b, c, 2013a).

The neural activation component converts incoming CSTs into the resulting twitch response triggered in the innervated muscle fibers using a critically damped, linear, second-order, differential system (Milner-Brown et al. 1973). This can be expressed in a discrete form using a time history-dependent, infinite impulsive response filter (Lloyd and Besier 2003):

$$u(t) = \alpha \cdot x(t - d) - \beta_1 \cdot u(t - 1) - \beta_2 \cdot u(t - 2) \tag{1}$$

where x(t) is the motor neuron spike train at time sample t, u(t) is the innervated fiber twitch response whereas α, β_1, β_2 are the recursive filtering coefficients. These are constrained to obtain a filter positive stable solution and unit gain: $\beta_1 = C_1 + C_2$, $\beta_2 = C_1 \cdot C_2$, $\alpha - \beta_1 - \beta_2 = 1$, with $-1 < C_1, C_2 < 0$. The term d is the electromechanical delay. The resulting u(t) is further processed via a nonlinear transfer function to compute the resulting neural activation:

$$a(t) = \frac{e^{Au(t)} - 1}{e^{A} - 1}, \tag{2}$$

where $-3 < A < 0$ is the non-linear shape factor, with 0 being a linear relationship. Neural activation a(t) reflects the ensemble dynamics of all electro-chemical transformations triggered at the muscle fiber level by the motor neuron discharges (Sartori et al. 2016).

The musculotendon kinematics component synthetizes subject-specific musculoskeletal geometry (e.g., MTU length and moment arms) into a set of MTU-specific

multidimensional cubic B-splines (Sartori et al. 2012c). Each B-spline computes MTU kinematics (i.e., MTU length and moment arms) as a function of input joint knee and ankle angles (Sartori et al. 2012c).

The musculotendon dynamics component uses neural activation and MTU length ℓ^{mt} and velocity v^{mt} to control a Hill-type muscle model and estimate instantaneous length, contraction velocity, and force in the muscle fibers, as well as strain and force in the series-elastic tendon within each MTU (Sartori et al. 2012a, 2013a).

The static properties of muscle fibers are modelled using parallel force–length passive $f_P\left(\widetilde{l}^m\right)$ and activation-dependent $f_A\left(\widetilde{l}^m\right)$ curves (Lloyd and Besier 2003). The dynamic properties of fibers are modelled using an activation-dependent force–velocity $f(\widetilde{v}^m)$ curve. These curves are normalized to maximum isometric muscle force ($F^{\max}$), while $\widetilde{l}^m$ and $\widetilde{v}^m$ represent fiber length and velocity normalized to optimal fiber length l_O^m and maximum muscle contraction velocity respectively (Zajac 1989). The tendon properties are modelled using a force-strain function $f(\varepsilon)$ with non-linear toe region normalized to $F^{\max}$ (Zajac 1989). The total MTU force F^{MTU} is calculated as a function of $a(t)$, normalized fiber length $\widetilde{l}^m$ and contraction velocity $\widetilde{v}^m$:

$$F^{MTU} = F^t = F^m \cos\left(\phi\left(l^m\right)\right) = \left\lfloor a(t) f\left(\widetilde{l}^m\right) f\left(\widetilde{v}^m\right) + f_P\left(\widetilde{l}^m\right) \right\rfloor F^{\max} \cos\left(\phi\left(l^m\right)\right) \tag{3}$$

2.1 From α-Motor Neurons Discharges to Muscle–Tendon Stiffness

The total stiffness K_i^{MTU} in each MTU can be modelled as muscle fiber stiffness K^m in series with tendon stiffness K^t (Sartori et al. 2015):

$$K^{MTU} = \left(\frac{1}{K^m} + \frac{1}{K^t}\right)^{-1} \tag{4}$$

Tendon stiffness K^t can be estimated from the slope of the non-linear force-strain relationship $f(\varepsilon)$ in the correspondence of the instantaneous tendon strain value ε. The tendon strain can be calculated at each simulation frame by solving for equilibrium between tendon and fiber force in the MTU dynamics equation (Eq. 3). Muscle fiber stiffness K^m is calculated as the partial derivative of fiber force F^m (Eq. 3) with respect to the normalized fiber length $\widetilde{l}^m$:

$$K^m = \frac{\partial F^m\left(a, \widetilde{l}^m, \widetilde{V}^m\right)}{\partial \widetilde{l}^m} \tag{5}$$

The partial derivative in Eq. 4 is calculated by creating a multi-dimensional cubic B-spline function per muscle (Sartori et al. 2015).

2.2 α-Motor Neurons Regulation of Joint Torque and Stiffness

Net joint moments are directly computed as the product of each MTU force (Eq. 3) and their associated moment arms from the MTU kinematics block. The net stiffness about a joint DOF, K^{DOF}, is determined as:

$$K^{DOF} = \sum_{i=1}^{\#MTU} K_i^{MTU} \cdot r_i^2 + \frac{\partial r_i}{\partial \theta^{DOF}} \cdot F_i^{MTU} \tag{6}$$

where K_i^{MTU} and r_i respectively represent the stiffness and moment arm of the ith MTU spanning the specific DOF, whereas θ^{DOF} is the joint angle about the specific DOF, as previously described (Sartori et al. 2015).

Previous research showed that the proposed neural data-driven modelling method could translate motor neuron spike trains into accurate joint moments in an open-loop way (Sartori et al. 2017a, b). This demonstrated the ability of establishing subject-specific modelling formulations that could convert neural activity from high-dimensional sets of motor neurons (on average 56.7 ± 10.2 for all muscles) into multi-muscle coordinated force profiles that well reconstruct experimental joint moments over all subjects and conditions (Fig. 2a).

These studies showed that that the effective part of the cumulative spike train responsible for force modulation was in the low frequency band (Negro and Farina 2011; Dideriksen et al. 2012; Sartori et al. 2017b). This was represented via slow neural activation profiles i.e., motor neuron spike trains filtered via a second-order twitch model. The direct association found between neural activation and joint moment is explained by the fact that the musculoskeletal system acts as a natural low pass filter of the spinal segments neural output. The neural drive high frequency band is filtered out by the slow twitch response of muscle fibers triggering electro-chemical transformations (i.e., calcium dynamic) and inducing limits in fiber action potential propagation velocity as well as by intrinsic viscoelasticity properties of muscle–tendon units (Enoka 2004).

Recent research proposed musculoskeletal models for estimating dynamic knee-ankle stiffness from muscle forces (Sartori et al. 2015). These studies suggested that the ankle joint modulates stiffness for accelerating or decelerating the body with co-contraction transitioning from dominant dorsi-flexors to dominant plantar-flexors throughout the stance phase of walking and running. On the other hand, knee joint stiffness appeared to be modulated for optimizing body weight acceptance and joint stability with more distributed co-contraction between flexor and extensor muscles

in the correspondence of the stiffness peaks produced during walking and running (Fig. 2b).

3 Conclusion

This chapter proposed the use of multi-muscle high-density EMG sampling and decomposition in combination with subject-specific neuromechanical modelling. This enables opening up a window into spinal motor neuron behavior and resulting mechanical function in vivo in the intact moving human.

References

Barbeau, H., McCrea, D. A., & O'Donovan, M. J., et al. (1999). Tapping into spinal circuits to restore motor function.

Bizzi, E., Cheung, V. C. K., & d'Avella et al. (2008). Combining modules for movement. *Brain Research Reviews, 57,* 125–133. https://doi.org/10.1016/j.brainresrev.2007.08.004.

Del Vecchio, A., Negro, F., Felici, F., & Farina, D. (2017). Distribution of muscle fiber conduction velocity for representative samples of motor units in the full recruitment range of the tibialis anterior muscle. *Acta Physiologica.* https://doi.org/10.1111/apha.12930.

Dideriksen, J. L., Negro, F., Enoka, R. M., & Farina, D. (2012). Motor unit recruitment strategies and muscle properties determine the influence of synaptic noise on force steadiness. *Journal of Neurophysiology, 107,* 3357–3369. https://doi.org/10.1152/jn.00938.2011.

Duchateau, J., & Enoka, R. M. (2016). Neural control of lengthening contractions. *Journal of Experimental Biology, 219,* 197–204. https://doi.org/10.1242/jeb.123158.

Enoka, R. M. (2008). *Neuromechanics of human movement*, 4th edn. Human KineticsPublishers, Inc.

Enoka, R. M. (2004). Biomechanics and neuroscience: A failure to communicate. *Exercise and Sport Sciences Reviews, 32,* 1–3. https://doi.org/10.1097/00003677-200401000-00001.

Enoka, R. M., & Pearson, K. G. (2013). *The motor unit and muscle action.* Princ neural Sci 768–789.

Farina, D., & Negro, F. (2015). Common synaptic input to motor neurons, motor unit synchronization, and force control. *Exercise and Sport Sciences Reviews,*, 43. https://doi.org/10.1249/JES.0000000000000032.

Farina, D., Vujaklija, I., Sartori, M., et al. (2017). Man/machine interface based on the discharge timings of spinal motor neurons after targeted muscle reinnervation. *Nature Biomedical Engineering 1,* 0025. https://doi.org/10.1038/s41551-016-0025.

Gogeascoechea, A., Kuck, A., Van Asseldonk, E., Negro, F., Buitenweg, J. R., Yavuz, U. S., Sartori M. (2020). Interfacing with alpha motor neurons in spinal cord injury patients receiving transspinal electrical stimulation. *Frontiers in neurology.* https://doi.org/10.3389/fneur.2020.00493. https://www.ncbi.nlm.nih.gov/pmc/articles/PMC7296155/

Gonzalez-Vargas, J., Sartori, M., Dosen, S., et al. (2015). A predictive model of muscle excitations based on muscle modularity for a large repertoire of human locomotion conditions. *Frontiers in Computational Neuroscience, 9,* 1–14. https://doi.org/10.3389/fncom.2015.00114.

Herzog, W. (2014). Mechanisms of enhanced force production in lengthening (eccentric) muscle contractions. *Journal of Applied Physiology, 116,* 1407–1417. https://doi.org/10.1152/japplphysiol.00069.2013.

Herzog, W., Powers, K., Johnston, K., & Duvall, M. (2015). A new paradigm for muscle contraction. *Front Physiol, 6,* 1–11. https://doi.org/10.3389/fphys.2015.00174.

Lee, D. D., & Seung, H. S. (1999). Learning the parts of objects by non-negative matrix factorization. *Nature, 401,* 788–791. https://doi.org/10.1038/44565.

Lloyd, D. G., & Besier, T. F. (2003). An EMG-driven musculoskeletal model to estimate muscle forces and knee joint moments in vivo. *Journal of Biomechanics, 36,* 765–776. https://doi.org/10.1016/S0021-9290(03)00010-1.

Milner-Brown, H. S., Stein, R. B., & Yemm, R. (1973). Changes in firing rate of human motor units during linearly changing voluntary contractions. *Journal of Physiology, 230,* 371–390.

Negro, F., & Farina, D. (2011). Linear transmission of cortical oscillations to the neural drive to muscles is mediated by common projections to populations of motoneurons in humans. *Journal of Physiology, 589,* 629–637. https://doi.org/10.1113/jphysiol.2010.202473.

Negro, F., Şükrü Yavuz, U., & Farina, D (2016). The human motor neuron pools receive a dominant slow-varying common synaptic input. *The Journal of Physiology*, 1–45. https://doi.org/10.1113/JP271748.

Sartori, M., Fernandez, J. W., & Modenese, L. et al. (2017a). Toward modeling locomotion using electromyography-informed 3D models: application to cerebral palsy. *WIREs System Biology Medicine*, e1368. https://doi.org/10.1002/wsbm.1368.

Sartori, M., Gizzi, L., Lloyd, D. G., & Farina, D. (2013a). A musculoskeletal model of human locomotion driven by a low dimensional set of impulsive excitation primitives. *Frontiers in Computational Neuroscience*, 7.

Sartori, M., Gizzi, L., Lloyd, D. G. D. G., & Farina, D. (2013b). A musculoskeletal model of human locomotion driven by a low dimensional set of impulsive excitation primitives. *Frontiers in Computational Neuroscience, 7*, 79. https://doi.org/10.3389/fncom.2013.00079.

Sartori, M., Llyod, D. G., & Farina, D. (2016). Neural Data-driven Musculoskeletal Modeling for Personalized Neurorehabilitation Technologies. *IEEE Transactions on Biomedical Engineering, 63,* 879–893. https://doi.org/10.1109/TBME.2016.2538296.

Sartori, M., Maculan, M., Pizzolato, C., et al. (2015). Modeling and Simulating the Neuromuscular Mechanisms regulating Ankle and Knee Joint Stiffness during Human Locomotion. *Journal of Neurophysiology, 114,* 2509–2527. https://doi.org/10.1152/jn.00989.2014.

Sartori, M., Reggiani, M., Farina, D., & Lloyd, D. G. (2012a). EMG-driven forward-dynamic estimation of muscle force and joint moment about multiple degrees of freedom in the human lower extremity. *PLoS One, 7*, 1–11. https://doi.org/10.1371/journal.pone.0052618.

Sartori, M., Reggiani, M., Pagello, E., & Lloyd, D. G. (2012). Modeling the human knee for assistive technologies. *IEEE Transactions on Biomedical Engineering, 59,* 2642–2649. https://doi.org/10.1109/TBME.2012.2208746.

Sartori, M., Reggiani, M., van den Bogert, A. J., & Lloyd, D. G. (2012). Estimation of musculotendon kinematics in large musculoskeletal models using multidimensional B-splines. *Journal of Biomechanics, 45,* 595–601. https://doi.org/10.1016/j.jbiomech.2011.10.040.

Sartori, M., Yavuz, U. S., & Farina, D. (2017). In Vivo Neuromechanics: Decoding Causal Motor Neuron Behavior with Resulting Musculoskeletal Function. *Scientific Reports, 7,* 13465. https://doi.org/10.1038/s41598-017-13766-6.

Zajac, F. E. (1989). Muscle and tendon: Properties, models, scaling, and application to biomechanics and motor control. *Critical Reviews in Biomedical Engineering, 17,* 359–411.